Published in final edited form as:
Acta Biomater. 2013 December ; 9(12): . doi:10.1016/j.actbio.2013.08.017.

Micropatterned Dermal-Epidermal Regeneration Matrices Create Functional Niches that Enhance Epidermal Morphogenesis

Amanda L. Clement[a,b], **Thomas J. Moutinho Jr.**[a,b], and **George D. Pins**[a,b]

[a]Biomedical Engineering Department, Worcester Polytechnic Institute, Worcester, Massachusetts 01609

[b]Bioengineering Institute, Worcester Polytechnic Institute, Worcester, Massachusetts 01609

Abstract

Although tissue engineered skin substitutes have demonstrated some clinical success for the treatment of chronic wounds such as diabetic and venous ulcers, persistent graft take and stability remain concerns. Current bilayered skin substitutes lack the characteristic microtopography of the dermal-epidermal junction that gives skin enhanced mechanical stability and creates cellular microniches that differentially promote keratinocyte function to form skin appendages and enhance wound healing. We developed a novel micropatterned dermal-epidermal regeneration matrix (μDERM) which incorporates this complex topography and substantially enhances epidermal morphology. Here, we describe the use of this 3D *in vitro* culture model to systematically evaluate different topographical geometries, to determine their relationship to keratinocyte function. We identified three distinct keratinocyte functional niches: the proliferative niche (narrow geometries), the basement membrane protein synthesis niche (wide geometries) and the putative keratinocyte stem cell niche (narrow geometries and corners). Specifically, epidermal thickness and keratinocyte proliferation is significantly ($p<0.05$) increased in 50 and 100 μm channels while laminin-332 deposition is significantly ($p<0.05$) increased in 400 μm channels compared to flat controls. Additionally, $\beta_1^{bri}p63^+$ keratinocytes, putative keratinocyte stem cells, preferentially cluster in channel geometries (similar to clustering observed in native skin) compared to a random distribution on flats. This study identifies specific target geometries to enhance skin regeneration and graft performance. Furthermore, these results suggest the importance of μDERM microtopography in designing next generation skin substitutes. Finally, we anticipate that 3D organotypic cultures on μDERMS will provide a novel tissue engineered skin substitute for *in vitro* investigations of skin morphogenesis, wound healing and pathology.

1. INTRODUCTION

Annually, three to four million diabetic and venous ulcers require clinical intervention [1]. In addition to profoundly impacting patient quality of life, the cost of treatment for venous and pressure ulcers exceeds $8 billion USD per year [1, 2]. With the average age of the population and the incidence of diabetes on the rise, these numbers are expected to increase,

Address Correspondence to: George D. Pins, PhD, Department of Biomedical Engineering, Worcester Polytechnic Institute, Worcester, MA 01609, Tel: 1-508-831-6742; Fax: 1-508-831-5541, gpins@wpi.edu.

CONFLICT OF INTEREST

The authors state no conflict of interest.

leading to a demand for wound closure products such as skin substitutes [1–3]. Tissue engineered skin substitutes represent a promising therapy option and have had limited clinical success, however there remains a significant clinical need for a robust tissue engineered skin substitute that reduces healing time while eliminating mechanically induced graft failure [1, 2, 4–7].

Skin, a complex multilayered tissue, is primarily responsible for maintaining a highly regulated semi-permeable barrier between the body and the environment [8]. Following traumatic disruption of the skin, rapid restoration of the barrier function is the first line of defense against infection and dehydration is critical for a ensuring a positive clinical outcome [1]. To better under the cellular mechanisms which direct these tissue responses, several groups have developed *in vitro* models of native skin [9–11]. While these models elucidate mechanisms that guide epidermal regeneration, they are limited in their capacity to precisely analyze the key topographic and biochemical roles of keratinocyte microniches at the dermal-epidermal junction (DEJ) in directing critical wound healing processes.

In native skin, the topography of keratinocyte microniches at the DEJ plays a critical role in maintaining the structure and mechanical properties of the tissue, as well as in directing its regenerative potential [12–14]. The DEJ is characterized by fingerlike dermal papillae (DP) and epidermal rete ridges that conform to the dermal topography. These features create microniches with dimensions ranging from 50–400 μm width and 50–200 μm depths [15, 16]. This interdigitated topography increases the surface area between the dermis and the epidermis, enhancing both the mechanical shear resistance of the skin and the paracrine diffusion between layers. Additionally, microtopographic niches create distinct cellular microenvironments that differentially direct keratinocyte phenotype and cellular function. For example, multiple labs demonstrated that keratinocyte stem cells preferentially locate to the tips of the DP or the bases of the rete ridges, depending on their anatomical location [13, 14, 17–19]. Interestingly, changes in DEJ topography are noted in skin diseases such as psoriasis (lengthening of rete ridges) and in aged skin (flattening of the DEJ), further suggesting an important role for topography in epidermal function [20, 21]. To further investigate the roles of 3D microniches on keratinocyte functions, several groups developed in vitro models to characterize the effects of cell geometries and surface chemistries on keratinocyte function [22–25]. However, a greater understanding of how 3D topographic, biochemical and cellular cues direct keratinocyte proliferation and cellular function will further our understanding of epidermal morphogenesis and skin wound healing and will allow us to harness these cues to develop the next generation skin substitutes.

Keratinocyte stem cells remain a controversial area of research with ongoing debate surrounding epidermal stem cell models as well as specific locations and appropriate markers for epidermal stem cells. Some of this confusion originates from the heterogeneous nature of the epidermal stem cell population. The epidermis contains several distinct stem cell populations, including interfollicular (IF) stem cells, hair follicle stem cells and sebaceous gland stem cells, which support epidermal maintenance and tissue regeneration [26]. These physical microniches contain several distinct keratinocyte sub-populations located throughout the epidermis, including both keratinocyte stem cells and terminally committed keratinocytes. In particular, evidence suggests that basal keratinocytes, once considered a homogenous population, represent a heterogeneous cell reservoir. Studies of native skin demonstrated clustering of phenotypically similar keratinocytes. Lavker and Sun suggested the existence of two spatially segregated keratinocyte subpopulation: nonserrated, slow-cycling keratinocytes located at the base of deep rete ridges and serrated keratinocytes located in shallow rete ridges [13, 14]. Later, Watt *et al.* examined stem cell patterning in the IF epidermis by correlating the regional variation in integrin expression levels in human skin with the colony forming efficiency of keratinocytes [12, 17–19]. Additionally, a recent study

of keratinocytes seeded on a microfabricated dermal papilla template showed differential gene expression on micropatterned membranes compared to flat controls [27]. Given the continued lack of understanding of the role of microtopography in directing cellular phenotype, function and fate, we suggest that the topography of the dermal-epidermal junction is largely responsible for driving the clustering of these keratinocyte sub-populations and hypothesize that topographical cues can be used to direct keratinocyte phenotype and create stem cell reservoirs. Further, we propose that μDERMs provide a novel platform for systematically investigating the roles of microtopography on cellular function as well as diverse keratinocyte stem cell niches.

In this manuscript, we investigated the influence of cellular microniche topography on keratinocyte function. We recently described a method to create micropatterned dermal-epidermal regeneration matrices (μDERMs) that facilitate the investigation of cellular responses to microtopographies [28]. In this study, we integrated fibroblast co-culture into our model system and specifically probed the formation of distinct proliferative and synthetic niches within micropatterned keratinocyte microniches. We demonstrated that keratinocytes in narrower channels exhibit a more proliferative phenotype, while keratinocytes in wider channels exhibit enhanced synthesis of the basement membrane (BM) protein laminin-332. Additionally, keratinocytes exhibiting the putative stem cell markers β_1 integrin and p63 preferentially localized to the base of narrow channels and the corners of wider channels. This novel approach to creating 3D model systems with topographical cues that mimic native cellular compartments at the DEJ will enable systematic investigation of the biophysical and biochemical cues that direct cutaneous tissue morphogenesis, epidermal pathologies.

2. Materials and Methods

2.1 Cell culture and media formulations

Neonatal primary human foreskin keratinocytes (NHKs) and primary human foreskin fibroblasts (NHFs) were isolated from foreskins, obtained as non-identifiable discard tissue from the University of Massachusetts Memorial Medical Center (Worcester, MA), and were approved with exempt status from the New England Institutional Review Board, using previously described methods. Prior to seeding on μDERMs, keratinocytes were cultured on a feeder layer of mitomycin C treated J2s (generously donated by Dr. Stelios Andreadis, State University of New York at Buffalo, Buffalo, NY). NHF medium consisted of Dulbecco's modified Eagle's medium (DMEM) with 10% fetal bovine serum (FBS) and 1% penicillin-streptomycin. HKF medium was comprised of a 3:1 blend of high glucose DMEM and Ham's F12 with 10% fetal bovine serum and 1% penicillin-streptomycin supplemented with adenine (1.8×10^{-14} M), cholera toxin (10^{-10} M), hydrocortisone (0.4 μg/ml), insulin (5 μg/ml), transferring (5 μg/ml), and triiodo-L-thyronine (2×10^{-9} M). After initial NHK plating, medium was replaced with NHK medium containing 10 ng/ml epidermal growth factor (EGF). Seeding medium for μDERM culture consisted of a 3:1 blend of high glucose DMEM and Ham's F12 with 1% fetal bovine serum and 1% penicillin-streptomycin supplemented with cholera toxin (10^{-10} M), hydrocortisone (0.2 μg/ml), insulin (5 μg/ml) and ascorbic acid (50 μg/ml). Priming medium consisted of seeding medium supplemented with 24 μM BSA, 25 μM oleic acid, 15 μM linoleic acid, 7 μM arachidonic acid, 25 μM palmitic acid, 10 μM L-carnitine, and 10 mM L-serine). Air-liquid interface (A/L) medium was serum-free priming medium supplemented with 1 ng/ml EGF.

2.2 In vitro μDERM culture model

2.2.1 μDERM Specifications—The microtopographic features of our μDERMs were designed specifically to enable concurrent histological evaluation of multiple geometries on

a single construct, to minimize experimental variations and analysis time. Specifically, 1.25 cm × 2.0 cm patterns were designed with 3 series of parallel channels 200 μm deep, 2500 μm long and with variable widths (50μm, 100μm, 200μm or 400μm). For histological analysis, μDERMs were sectioned perpendicular to the channels to provide multichannel analysis on each section.

2.2.2 μDERM Fabrication—μDERM fabrication was modified from a previous method [28] by incorporating fibroblasts into the dermal sponge and decreasing the thickness of the collagen gel-matrix (Figure 1). Specifically, a pattern was designed with a series of 200μm deep channels with varying widths (50μm, 100μm, 200μm, 400μm) [28, 29]. Type I acid-soluble collagen (10 mg/ml in 5 mM HCl) was purified from rat tail tendons [30, 31] and 0.3 ml of this collagen solution was self-assembled on the micropatterned molds using 5x DMEM (Invitrogen) with 0.22 M $NaHCO_3$ and 0.1 M NaOH (Sigma) for 18 hours at 37°C and 10% CO_2. To construct a dermal analog, following polymerization a collagen-GAG sponge was laminated to the back of the micropatterned gel using an additional 0.3 ml of self-assembled collagen and then crosslinked with EDC. μDERMs were then removed from the PDMS patterns and conjugated with fibronectin (FN). μDERMs were sterilized in an antibiotic cocktail (100 IU/ml-100μg/ml penicillin-streptomycin, 2.5μg/ml amphotericin B, 10pg/ml ciprofloxacin, 100μg/ml gentamycin) for a minimum of 24 hours at room temperature and rinsed with DMEM.

2.2.3 Cell Seeding and *in vitro* Culture of μDERMs—For cell seeding, μDERMs were placed on custom-designed cell seeding screens (Figure 1 K,L). Medical grade 316 stainless steel screens were embedded in PDMS platforms, leaving the center of the screen open. These PDMS platforms elevated the screens to allow for culture at the air-liquid interface. Initially, 8×10^4 NHFs/cm^2 in 100μl of NHF medium were seeded on the dermal side of the scaffold and incubated for 2 hours. Following incubation, additional fibroblast medium was added, and μDERMs were cultured for 48 hours (37°C, 10%CO_2) with daily medium changes (Figure 1H). μDERMs were inverted onto A/L screens, NHKs were seeded on the micropatterned side at a density of 5×10^5 cells/cm^2 in 100μl seeding medium for 2 hours then μDERMs were submerged in seeding medium(Figure 1I). As a control, de-epidermized dermis (DED) was seeded with keratinocytes and cultured alongside μDERMs, as previously described [28]. After 24 hours, seeding medium was replaced with priming medium for 48 hours. Finally, priming medium was replaced with A/L interface medium and μDERMs were cultured for 3 or 7 days at the A/L interface (Figure 1 M).

2.3 Quantitative Morphometric Evaluation of Cultured μDERMs

μDERMs were fixed in neutral buffered formalin, embedded in Paraplast (McCormick Scientific) and sectioned perpendicular to the microchannel topography. Slides were stained with hematoxylin and eosin (Richard Allen Scientific). Channel depth, channel width, epidermal thickness in the channel and epidermal thickness on the neighboring plateaus were measured for each channel using Spot software (Figure 3A). For each well, channel depth and epidermal thickness were measured in 3 locations (center and each side) and then averaged to determine channel depth and epidermal thickness. Channel width was measured in 3 places (bottom, top and center) and then averaged to determine channel width. To account for variations in μDERM dimensions, the average epidermal thickness was normalized to the average channel depth of the corresponding well. Plateau thickness was measured immediately adjacent to either side of each channel and then averaged to determine the adjacent plateau thickness (Figure 3B). Each μDERM section contained up to 4 replicates of each channel geometry. For each geometry, channels were analyzed on at least 3 separate μDERMs. Sample sizes for normalized epidermal thickness measurements were n=7, 9, 14 and 15, for 3 days of culture (50μm, 100μm, 200μm and 400μm channel

widths, respectively); n= 19, 19, 19, and 21, for 7 days of culture with fibroblasts (50μm, 100μm, 200μm and 400μm channel widths, respectively); and n = 4, 5, 3, and 8, for 7 days of culture without fibroblasts (50μm, 100μm, 200μm and 400μm channel widths, respectively). Sample sizes for plateau thickness measurements were n=21, 14, 18, 28, 30, for 3 days of culture (flats, 50μm, 100μm, 200μm and 400μm channel widths, respectively); n= 21, 40, 38, 38, 40, for 7 days of culture with fibroblasts (flats, 50μm, 100μm, 200μm and 400μm channel widths, respectively);and n = 9, 6, 10, 6, 16, for 7 days of culture without fibroblasts (flats, 50μm, 100μm, 200μm and 400μm channel widths, respectively). Epidermal thickness of DED and native foreskin tissue was also measured. Finally, individual channels with mean geometries that deviated from the population mean values by more than two standard deviations were excluded from analysis.

2.4 Immunohistochemistry (IHC)

To further evaluate the similarities between our 3D scaffolds and the experimental controls, immunohistochemical analysis was performed on 7 day cultures of μDERMs containing fibroblasts.

2.4.1 Laminin-332 Immunohistochemistry—Laminin-332 was detected by staining for the laminin γ_2 chain, using methods based on those described previously [32, 33]. Briefly, following antigen retrieval (Protease XXIV, 15 minutes) and blocking (5% skim milk in PBS, 10 minutes) sections were incubated with laminin γ_2 antibody diluted (1:200 in blocking solution; D4B5, Millipore) overnight at 4°C. Subsequently, sections were incubated with AlexaFluor546 secondary goat-anti-mouse antibody (Invitrogen). Negative control samples were incubated with blocking buffer, in lieu of primary antibody.

2.4.2 Ki67, β_1 integrin and p63 Immunohistochemistry—Antigen retrieval for ki67, β_1 integrin and p63 IHC was performed by boiling paraffin section on slides in a citrate buffer as previously described [28]. Sections were blocked in 10% horse serum for 10 minutes and then incubated with either mouse-antihuman CD29 antibody (β_1 integrin; BioGenex) and rabbit-antihuman p63 antibody (H-137, Santa Cruz) overnight at 4°C or with prediluted mouse-antihuman Ki67 antibody (Zymed) overnight at room temperature. Subsequently, sections were incubated with both AlexaFluor546 (Invitrogen) secondary goat-anti-mouse antibody and AlexaFluor 488 (Invitrogen) secondary donkey-anti-rabbit antibody (β_1 integrin and p63) or with AlexaFluor 546 alone (ki67). Negative control samples were incubated with blocking buffer, in lieu of primary antibody. Foreskin tissue was used as a positive immunohistochemistry control.

2.5 Statistical Analysis

Statistical differences were evaluated using SigmaPlot Version 11.0 (Systat Software, Inc.). 1-Way Analysis of Variance (ANOVA) and 2-Way ANOVA were performed to determine statistical differences, as indicated. For comparisons between groups, Holm-Sidak post-hoc analysis was performed. For keratinocyte proliferation studies, Dunnett's method was used for post-hoc analysis to compare μDERM conditions to foreskin controls. For all comparisons, a significant difference between groups was indicated by a p value < 0.05.

3. RESULTS

In this study, we incorporated fibroblasts in the dermal sponge component of our *in vitro* μDERM model system (Figure 1) and we analyzed the effect of microniche topography, fibroblast signaling and culture time on epidermal thickness and stratified morphology. We also examined changes in keratinocyte proliferation and laminin-332 synthesis as a function

of microniche topography and assessed clustering of the $\beta_1^{bri}p63^+$ keratinocyte phenotype in microtopographies.

3.1. Microtopography and fibroblasts enhance epidermal morphology and increase epidermal thickness

NHFs were incorporated into the 3D *in vitro* μDERM culture model to establish keratinocyte responses that more closely mimicked the native tissue microenvironments. μDERMs cultured with fibroblasts (Figure 2, Columns 1 and 2) exhibited increased epidermal thickness and enhanced epidermal morphology, including a more robust basal layer, compared to μDERMs cultured without fibroblasts (Figure 2, Column 3). This model system provides a more physiologic model to study the effect of microtopography on epidermal morphology and keratinocyte function.

3.1.1 Morphological Assessment of Cultured μDERMs—Our fabrication process (Figure 1) yielded a μDERM with a collagen gel matrix ranging in average thickness from 87 μm (beneath channels) to 186 μm (plateaus) and collagen dermal sponges 336 μm thick. The average thickness of the flat collagen gel matrix was 129 μm. Keratinocyte stratification in channels (50μm, 100μm, 200μm and 400μm in width; 200 μm in depth) and flat regions of μDERMs containing fibroblasts was evaluated following 3 and 7 days of culture at the air-liquid interface (A/L) (Figure 2, Columns 1 and 2). In μDERMs containing fibroblasts, scaffolds contain distinctly stratified epidermal morphology, which closely recapitulates the morphologies observed on neonatal foreskin tissue controls and keratinocyte-seeded, DED scaffold controls (Figure 2 row 6). In μDERMs with channels, four distinct, stratified keratinocyte layers can be observed in the epidermal layer by 7 days of A/L culture. We also observed an increase in stratification in regions of the graft containing topographic features (50μm, 100μm, 200μm, and 400μm channels) compared to in flat regions (Figure 2 M, O). These regions of the grafts exhibit pronounced stratum granulosum layers comparable to native skin tissue (Figure 2R), regardless of channel dimension. In contrast, intermediate stratum granulosum and spinosum layers are not readily distinguished in comparable flat regions of control grafts. At 3 days, epidermal stratification is limited to the stratum corneum and a partially organized basal layer.

3.1.2 Quantitative Morphometric Analysis of Normalized Epidermal Thickness —To further characterize the effects of microtopography, we quantitatively assessed the thickness of the cultured epidermis in different microniche dimensions (Figure 3 A, B). Overall, normalized epidermal thickness is increased in narrow (50μm and 100μm) channels compared to wide (200μm and 400μm channels). At 3 days, the normalized epidermal thickness in 50μm and 100μm channels is statistically increased compared to wider 200μm and 400μm channels ($p<0.05$, Figure 3C). This result persists at 7 days.

Consistent with the enhanced epidermal morphology noted in histological evaluations, epidermal thickness increased significantly between 3 and 7 days ($p<0.05$, Figure 3A, C). This trend of increased epidermal thickness was most pronounced in the 200μm and 400μm channels where thickness was increased by 35% and 65% respectively between 3 and 7 days. Epidermal thickness on plateaus was also thicker at 7 days ($p<0.05$, Figure 3D). Interestingly, in 400μm channels, epidermal thickness at 3 days does not exceed channel depth (normalized thickness < 1) (Figure 3B), resulting in an invagination on the surface of the stratum corneum (Figure 2J). By 7 days, epidermal thickness exceeded channel depth for all dimensions, including 400μm channels and surface depressions are not readily apparent.

3.1.3 Quantitative Morphometric Analysis of Epidermal Thickness on Plateaus in Proximity to Channels—We observed that the increased epidermal thickness on

μDERMs containing narrow channels was not limited to the channel itself but appeared to extend to the immediately adjacent shoulder regions. To evaluate this, we compared the thickness of the epidermis on flat plateaus immediately adjacent to microchannels (Figure 3A) to the thickness on control flat regions. Again, epidermal thickness increased significantly between 3 and 7 days of A/L culture, independent of topography ($p<0.05$). Interestingly, the presence of microtopography affected epidermal thickness on adjacent plateaus compared to control flat regions. When compared to flat regions, epidermal thickness was increased in regions adjacent to narrow channels and decreased in regions adjacent to wide channels (Figures 2, 3D). After 3 days in culture, epidermal thickness near 100μm channels and was significantly greater than the epidermal thickness on flat controls and on plateaus in proximity to all other channel dimensions. In contrast, epidermal thicknesses for proximal plateaus of wider 200μm and 400μm channels were decreased compared to flats; epidermal thickness adjacent to 400μm channels also decreased compared to 200μm channels. The results at 7 days were similar. Specifically, epidermal thickness on plateaus adjacent to 50μm channels was increased significantly compared to flat regions and plateaus adjacent to 200μm and 400μm channels, while epidermal thickness on proximal plateaus near 400μm channels decreased significantly compared to all other dimensions. At 7 days, plateau thicknesses on flats and near 50μm, 100μm and 200μm channels were comparable to epidermal thickness on DED and native foreskin tissue.

3.2 Microtopography directs the formation of distinct keratinocyte niches

3.2.1 The proliferative keratinocyte niche is located in regions with narrow microniches—To further analyze the mechanisms contributing to the increased epidermal thickness in and near narrow microniches, we analyzed the proliferative index of grafts cultured for 7 days using the proliferative marker ki67. Representative images are shown for the various microniche geometries in Figure 4A–F. The number of ki67+ cells/mm of DEJ length was calculated for each well dimension (Figure 4G). The number of ki67+ cells/mm was not statistically different on DED compared to μDERMs for all topographic dimensions, but 100 μm channels had a significantly increased density of ki67+ keratinocytes in the basal layer compared to 400 μm channels. It is also interesting to note that the ki67+ cell density in these wells was statistically comparable to the ki67+ cell density in native foreskin tissue.

A distinct feature of the μDERM surface is that it provides increased total surface area relative to flat, planar control scaffolds. To determine whether this increased surface area increases the ki67+ cell density, we measured the number of ki67+ cells/planar graft length (Figure 4H). Overall ki67+ keratinocyte density was increased in regions with 50μm channels compared to 200 and 400 μm channels, flat controls and DED controls. Additionally ki67+ keratinocyte density in regions with 50μm channels approximated the density in foreskin control. Taken together, these results suggest that narrow microniches enhance keratinocyte proliferation.

3.2.2 Basement membrane protein synthesis is enhanced in wider microniches—To investigate the effects of keratinocyte microniches on BM synthesis, scaffolds were analyzed after 7days of culture at the A/L. Histological sections were immunostained for laminin-332 (γ2 chain) and nuclei were counterstained with Hoechst (Figure 5 A–F). A continuous layer of laminin deposition was observed at the dermal-epidermal junction of all μDERM topographies, flat controls and DED. To visualize areas of increased laminin-332 deposition, false colorization was applied after background subtraction (blue = top 1/3 intensity, green = mid 1/3 intensity, and red = lowest 1/3 intensity normalized to the maximum intensity in the image set) (Figure 5G–L). To quantify laminin-332 deposition and distribution, the average relative fluorescence intensity/length of

laminin γ2 chain expression localized to the DEJ was determined for the plateaus, base and sides of each dimension. There was no significant difference in laminin deposition between regions of individual channels (plateaus, bases, and sides). However, overall laminin deposition was decreased in 50μm and 100μm channels compared to 200μm channels, 400μm channels and flats. In 400μm channels, laminin deposition was increased over flat controls and in both 400μm and 200μm channels, laminin deposition increased relative to DED controls. This suggests that wider keratinocyte niches promote a synthetic phenotype.

3.2.3 The β_1^{bri} $p63^+$ keratinocyte niche is located at the base of narrow microniches—To further examine the presence of distinct keratinocyte niches in μDERMs, we performed immunohistochemistry for β_1 integrin and p63 – putative keratinocyte stem cell markers (Figure 6). In suprabasal keratinocytes, β_1 integrin expression was low (bottom 1/3 brightness, β_1^{dim}) or completely absent. The majority of basal keratinocytes expressed moderate (middle 1/3 brightness, β_1^{mid}) or high (top 1/3 brightness, β_1^{bri}) levels of β_1 integrin. Additionally, p63 expression was predominately localized to the basal keratinocytes, with clusters of $p63^+$ cells overlapping clusters of β_1^{bri} cells. These clusters of $\beta_1^{bri}p63^+$ keratinocytes were located predominately in the bottoms of narrow 50μm and 100μm channels (Figure 6A and 6B) and in the corners of wide 200 μm and 400μm channels (Figures 6C and 6D). In contrast, $\beta_1^{bri}p63^+$ keratinocytes were randomly distributed within the basal layer of keratinocytes cultured on flat interfaces (Figure 6E). This suggests the ability of microtopography to sequester phenotypically similar keratinocytes.

4. DISCUSSION

Future innovations to skin substitutes necessitate the development of a 3D *in vitro* skin model that enables facile systematic evaluations of the effect of microtopographic features on keratinocyte function in cellular niches that mimic the physical topography of the DEJ. This study builds upon our μDERM model [28] to demonstrate that topographic features can drive keratinocyte compartmentalization into proliferative, synthetic and $\beta_1^{bri}p63^+$ keratinocyte niches. In this study, we found that epidermal thickness was increased in and near narrow channel geometries, suggesting that topographic features contribute to keratinocyte-mediated epidermal morphogenesis. Further, the density of $ki67^+$ keratinocytes was increased in cellular regions with narrow channel geometries, while the amount of laminin-332 deposited on μDERM surfaces was increased in regions with wide channels. Additionally, we found that $\beta_1^{bri}p63^+$ keratinocytes clustered in the bases of narrow channels and the corners of wider channels. Together, these results support the hypothesis that keratinocytes cultured on μDERM will aggregate into distinct cell subpopulations in response to topographic cues. These findings also suggest that, independent of biochemical cues, microtopography can be used to drive cellular function.

In nature, the epidermis conforms to the complex series of rete ridges and papillary plateaus of the DEJ, creating 3D biophysical and biochemical microniches that regulate keratinocyte phenotype and cellular functions. In this study, we seek to precisely recapitulate the keratinocyte microenvironments of the DEJ. Previously, we showed enhanced epithelialization when keratinocytes were cultured in narrow channel topographies on μDERMS surfaces, in the absence of fibroblasts [28, 29]. Recent studies showed that fibroblasts facilitate keratinocyte growth and differentiation via a double paracrine mechanism [34–36], as well as enhance re-epithelialization and improve the performance of skin substitutes [37–39]. Our new μDERM model incorporates fibroblasts into the dermal layer and creates a more biomimetic *in vitro* model system that enables the evaluation of the effect of microtopography on keratinocyte proliferation. While the mechanisms by which fibroblasts direct keratinocyte function are not completely understood, fibroblasts are known

to play a critical role in epidermal morphogenesis. Specifically, previous research demonstrates that the inclusion of fibroblasts stimulates keratinocyte proliferation and differentiation within the stratum granulosum [37, 40–42]. μDERMs co-cultured with fibroblasts were compared to μDERMs cultured without fibroblast to validate the effect of fibroblast paracrine signaling. Our observation that a thicker, more robust epidermal layer forms in the presence of fibroblasts, suggests that fibroblasts provide paracrine signals to enhance epidermal stratification within our model. Additionally, we see an enhanced stratum granulosum present in μDERM containing fibroblasts. These results are consistent with previous results demonstrating that fibroblast-keratinocyte paracrine signaling is critical for epidermal morphogenesis [37–39]

When keratinocytes were cultured on μDERMs in the presence of fibroblasts we observed a more robust epidermal layer with little evidence of structural disruptions at the DEJ. Interestingly, we also observed stable epidermal layers when we cultured cells on DED. One of the differences between μDERMS and DED is the complexity of the BM chemistry. Previous studies demonstrated that fibroblast-keratinocyte paracrine signaling is necessary for the synthesis and appropriate localization of BM proteins in skin [43, 44]. This supports the hypothesis that one of the roles of the fibroblasts is to enhance the synthesis of new BM on μDERMS. Additionally, the differences in epidermal thickness between topographic dimensions are more pronounced in μDERM containing fibroblasts. Keratinocyte growth factor (KGF), which is secreted by fibroblasts in fibroblast-keratinocyte co-cultures, is known to upregulate both keratinocyte proliferation and laminin-332 deposition [34]. In our μDERM model, we see a statistically significant increase in the number of proliferative keratinocytes in narrow channels compared to wide channels and flat controls. Importantly, in first generation μDERMs lacking fibroblasts there were no significant differences in $ki67^+$ cell density between channels of different dimensions [28]. However, an increase in laminin-332 deposition was demonstrated in wider channels. Since both proliferative and synthetic keratinocytes are essential for proper epidermal morphogenesis, DEJ topography may regulate these two functions as a response to soluble factors. In future studies we will further probe this by quantifying the effect of exogenous KGF on keratinocytes cultured in different microtopographies.

Our results with μDERMs containing fibroblasts suggest that microtopography contributes to modulating keratinocyte proliferation. These findings significantly augment our previously proposed space filling mechanism to explain increased epidermal thickness in narrow channels of keratinocyte microniches [28]. In our earlier studies on bioengineered skin substitutes containing microfabricated basal lamina analogs lacking fibroblasts, we observed a decrease in proliferating keratinocyte following initial seeding: first in narrow channels (3 days) and then in wide channels (7 days), and we found no statistically significant differences in ki67+ keratinocyte density in channels of different dimensions [28]. This led us to propose a space filling mechanism to explain the increased epidermal thickness in narrow channels. However, here we show that in μDERMs containing fibroblasts (after 7 days A/L), the density of proliferating cells along the DEJ is higher in narrow (100μm) channels. Further, the density of proliferating cells on the scaffold is also higher in narrow (50μm) channels. This suggests that channel topography can direct cellular proliferation and indicates that a space filling mechanism is not solely responsible for increased epidermal thickness. Previous work has demonstrated the importance of keratinocyte-fibroblast paracrine signaling to the maintenance of the proliferative keratinocyte phenotype. We hypothesized that the absence of fibroblast signaling in our previous work may have resulted in a quiescent phenotype, limiting our ability to fully investigate microtopographic cues. To address this limitation and to generate a more physiologically relevant model, we incorporated dermal fibroblasts into our μDERM model. Our results which demonstrate a thicker, more robust epidermal layer in the presence of

fibroblasts are consistent with previously published works and suggest that the incorporation of fibroblasts into our model system allows us to more explicitly probe the ability of microtopography to create distinct keratinocyte niches. Incorporating fibroblasts into the dermal sponge may be particularly important for future *in vivo* studies. A previous study using a murine transplantation model demonstrated that incorporation of fibroblasts into a composite skin substitute not only improved epidermal formation but also enhanced vascularization and reduced graft contraction *in vivo* [39].

We also examine the influence of microtopography on the deposition of the BM protein laminin-332 [45]. Importantly, keratinocytes seeded on μDERMs deposited a continuous layer of laminin-332 along the surfaces of all of the microniches at the DEJ. In quiescent skin, laminin-332 is part of the anchoring filaments at the DEJ and is essential for keratinocyte adhesion to the underlying dermis via the $\alpha_6\beta_4$ integrin [46–48]. Mutations in the genes coding for the laminin-332 subunits (LAMA3, LAMB3, and LAMC2) lead to junctional epidermolysis bullosa (JEB) which is characterized by severe blistering at the lamina lucida [49, 50]. Additionally, following skin wounding laminin-332 is secreted by epidermal keratinocytes to facilitate wound re-epithelialization [51–53]. We showed increased laminin synthesis was inversely related to proliferating keratinocyte density. In wide (200μm and 400μm) channels, laminin deposition was increased compared to narrow channels. In 400μm channels, laminin deposition was also increased compared to flat controls. This relationship suggests a synthetic keratinocyte niche exists in wide channels. Since both keratinocyte proliferation and BM deposition are critical for wound healing, these results suggest the importance of including microtopographic features of multiple dimensions in complete tissue engineered skin grafts.

Finally, we examine the influence of microtopography on the localization of the stem-like $\beta_1^{bri}p63^+$ keratinocyte population. We demonstrated clustering of these cells in the base of narrow channels and the corners of wide channels, supporting the role of cellular adhesion in keratinocyte stem cell maintenance. In native skin, keratinocyte stem cells are found to preferentially locate to the tips of the DP or the base of the rete ridges [13, 14, 17–19]. However, on flat skin substitutes, these cells are randomly distributed. The ability of μDERM to recreate this patterning *in vitro* provides an important platform for future studies. Further, the heterogeneity of β_1 integrin and p63 expression in basal keratinocytes and the clustering of $\beta_1^{bri}p63^+$ keratinocytes further supports the theory that distinct keratinocyte microniche topographies on μDERMs modulate keratinocyte function. These results suggest that μDERMs can promote stem cell clustering; however, given the controversy over epidermal stem cell markers and distinct stem cell populations, further evaluation is necessary. To further probe this clustering phenomenon and to better elucidate the feasibility of creating an *in vitro* stem cell niche, future studies will focus on isolating and characterizing keratinocytes from microniches for clonal analysis via microdissection. Importantly, the existence of a keratinocyte response to morphological cues may help explain the heterogeneous basal keratinocyte population that is observed as keratinocytes respond to their local microenvironments.

The mechanism by which microtopography promotes cell sequestering both *in vitro* and *in situ* is not completely understood. One hypothesis is that cell phenotype and function is driven by variable nutrient availability due to the diffusion and mass transport profile through the substrate. In the μDERM model, the channel bases are in closer proximity to the dermal sponge than the plateaus, which we hypothesize will result in a higher concentration of fibroblast secreted cytokines in channels compared to plateau regions. This may be partially responsible for the differences in cell function between channel regions, plateau regions and flats. However, the differences in laminin 332 deposition, keratinocyte proliferation, epidermal thickness and $\beta_1^{bri}p63^+$ keratinocyte localization between channels

of different dimensions suggest mass transport of paracrine signals through the collagen gel may not be the only mechanism involved in the keratinocyte response to microtopography. Differential oxygen diffusion through the keratinocyte layers may also create localized regions of hypoxia. Importantly, regional hypoxia is present in native skin, particularly in hair follicles and dermal glands [54]. *In vitro* studies have shown that keratinocytes grown under hypoxic conditions exhibit reduced laminin 332 synthesis [55]. Here we have demonstrated that keratinocytes grown in narrow channels generate a thicker epidermal layer and also exhibit reduced laminin 332 synthesis compared to wide channels and flat controls. The increased epidermal thickness may create regional hypoxia which results in a reduction of laminin synthesis. However, hypoxia alone cannot account for the differences in laminin 332 synthesis because laminin deposition in 400μm channels is increased compared to on flats, despite having a much thicker epidermal layer within the channel. Finally, microtopographic mechanical cues may drive cellular function through static compressive and tensile forces induced by the topography. Previously, Fratzl *et al.* demonstrated that geometric cues such as channel surface area and local substrate curvature influenced the rate of bone tissue growth[56]. It is likely that multiple microtopographic-mediated mechanisms are responsible for the observed phenomenon. Future studies will investigate the specific contributions of mass transport and nutrient diffusion, hypoxic gradients and static mechanical stresses on keratinocyte phenotype and function in an attempt to further elucidate the importance of the microtopographic environment of the DEJ.

By integrating microfabrication technologies into the biomaterials design process, this work provides a robust research platform which we began to use to conduct systematic analyses of the fundamental relationships between the precise dimensions of the 3D cellular microenvironments and keratinocyte functions that significantly enhance the regeneration of robust epidermal layers on the surfaces of our skin substitutes. One benefit of the μDERM platform is that the micropatterned tissue analog is implantable, making it versatile for future *in vivo* wound healing studies as well as *in vitro* assays. Using this platform, we will continue to identify design parameters for the clinical development of robust skin substitutes that would benefit the growing need for treatment of burns, chronic wounds and diabetic ulcers.

5. Conclusions

Our findings from this study suggest a key role for microtopography in the segregation and promotion of keratinocyte niches. Strategic selection of microtopographic features can be used to design more advanced engineered skin constructs targeted to specific functions for both *in vitro* models as well as for clinical use. To reach the full potential of microtopographic regulation of keratinocyte phenotype, further research is necessary to elucidate the mechanisms behind niche formation. In the future we plan to examine the temporal synthesis of different BM proteins and the development of barrier function on μDERM with different topographical geometries. Our findings suggest that these novel μDERMs will serve as a platform for the development of highly tailored tissue engineered skin substitutes for use in the treatment of full-thickness wounds and as an *in vitro* organ system to study skin morphogenesis, wound healing, epidermal pathologies and drug screening assays.

Acknowledgments

This research was funded by the NIH (EB-005645). The authors wish to thank Dr. Mehmet Toner and Octavio Hurtado at the BioMicroElectroMechanical Systems (BioMEMS) Resource Center, Massachusetts General Hospital, Boston, MA (NIH Grant: P41 EB02503 [MT]), for their assistance with the microfabrication processes. The authors would also like to thank Jen Sansom for her technical assistance, the Department of Obstetrics and Gynecology at UMMS (Worcester, MA) for providing us with neonatal foreskins for keratinocyte isolations and

Russell Kronengold, Ph.D., at the Kensey Nash Corporation (Exton, PA), for his generous donations of SEMED-S collagen.

References

1. Macri L, Clark RA. Tissue engineering for cutaneous wounds: selecting the proper time and space for growth factors, cells and the extracellular matrix. Skin Pharmacol Physiol. 2009; 22:83–93. [PubMed: 19188756]
2. Shevchenko RV, James SL, James SE. A review of tissue-engineered skin bioconstructs available for skin reconstruction. J R Soc Interface. 2010; 7:229–58. [PubMed: 19864266]
3. Carlson B. BioMarket Trends: Phalanx of Treatments Propels Burn Market: Recombinant Growth Factor Theapies Are Predicted to Be Up-and-Coming Players. Genetic Engineering and Biotechnology News. 2008
4. Boyce ST. Design principles for composition and performance of cultured skin substitutes. Burns. 2001; 27:523–33. [PubMed: 11451611]
5. Sheridan RL, Tompkins RG. Skin substitutes in burns. Burns. 1999; 25:97–103. [PubMed: 10208382]
6. Supp DM, Boyce ST. Engineered skin substitutes: practices and potentials. Clin Dermatol. 2005; 23:403–12. [PubMed: 16023936]
7. Auger FA, Lacroix D, Germain L. Skin substitutes and wound healing. Skin Pharmacol Physiol. 2009; 22:94–102. [PubMed: 19188757]
8. Rook, A.; Burns, T. Rook's textbook of dermatology. 8. Chichester, West Sussex, UK; Hoboken, NJ: Wiley-Blackwell; 2010. p. 1online resource (4 v.)
9. Gautrot JE, Wang C, Liu X, Goldie SJ, Trappmann B, Huck WT, et al. Mimicking normal tissue architecture and perturbation in cancer with engineered micro-epidermis. Biomaterials. 2012; 33:5221–9. [PubMed: 22541538]
10. Powell HM, McFarland KL, Butler DL, Supp DM, Boyce ST. Uniaxial strain regulates morphogenesis, gene expression, and tissue strength in engineered skin. Tissue Eng Part A. 2010; 16:1083–92. [PubMed: 19845460]
11. Bellas E, Seiberg M, Garlick J, Kaplan DL. In vitro 3D full-thickness skin-equivalent tissue model using silk and collagen biomaterials. Macromol Biosci. 2012; 12:1627–36. [PubMed: 23161763]
12. Jones PH, Harper S, Watt FM. Stem cell patterning and fate in human epidermis. Cell. 1995; 80:83–93. [PubMed: 7813021]
13. Lavker RM, Sun TT. Heterogeneity in epidermal basal keratinocytes: morphological and functional correlations. Science. 1982; 215:1239–41. [PubMed: 7058342]
14. Lavker RM, Sun TT. Epidermal stem cells. J Invest Dermatol. 1983; 81:121s–7s. [PubMed: 6190957]
15. Odland GF. The morphology of the attachment between the dermis and the epidermis. Anat Rec. 1950; 108:399–413. [PubMed: 14799878]
16. Fawcet, DW.; Jensh, RP. Concise Histology. New York, NY: Chapman and Hall; 1997.
17. Watt FM. Epidermal stem cells: markers, patterning and the control of stem cell fate. Philos Trans R Soc Lond B Biol Sci. 1998; 353:831–7. [PubMed: 9684280]
18. Watt FM. The stem cell compartment in human interfollicular epidermis. J Dermatol Sci. 2002; 28:173–80. [PubMed: 11912004]
19. Watt FM. Stem cell fate and patterning in mammalian epidermis. Curr Opin Genet Dev. 2001; 11:410–7. [PubMed: 11448627]
20. Murphy M, Kerr P, Grant-Kels JM. The histopathologic spectrum of psoriasis. Clin Dermatol. 2007; 25:524–8. [PubMed: 18021888]
21. Montagna W, Carlisle K. Structural changes in aging human skin. J Invest Dermatol. 1979; 73:47–53. [PubMed: 448177]
22. Charest JL, Jennings JM, King WP, Kowalczyk AP, Garcia AJ. Cadherin-mediated cell-cell contact regulates keratinocyte differentiation. J Invest Dermatol. 2009; 129:564–72. [PubMed: 18754040]

23. Trappmann B, Gautrot JE, Connelly JT, Strange DG, Li Y, Oyen ML, et al. Extracellular-matrix tethering regulates stem-cell fate. Nat Mater. 2012; 11:642–9. [PubMed: 22635042]
24. Gobaa S, Hoehnel S, Roccio M, Negro A, Kobel S, Lutolf MP. Artificial niche microarrays for probing single stem cell fate in high throughput. Nat Methods. 2011; 8:949–55. [PubMed: 21983923]
25. Gilbert PM, Blau HM. Engineering a stem cell house into a home. Stem Cell Res Ther. 2011; 2:3. [PubMed: 21345268]
26. Pincelli, C.; Marconi, A. Keratinocyte Stem Cells: Biology and Clinical Applications. In: Baharvand, H.; Aghdami, N., editors. Regenerative Medicine and Cell Therapy. Humana Press; 2013. p. 57-64.
27. Lammers G, Roth G, Heck M, Zengerle R, Tjabringa GS, Versteeg EM, et al. Construction of a microstructured collagen membrane mimicking the papillary dermis architecture and guiding keratinocyte morphology and gene expression. Macromol Biosci. 2012; 12:675–91. [PubMed: 22416023]
28. Bush KA, Pins GD. Development of microfabricated dermal epidermal regenerative matrices to evaluate the role of cellular microenvironments on epidermal morphogenesis. Tissue engineering Part A. 2012; 18:2343–53. [PubMed: 22724677]
29. Downing BR, Cornwell K, Toner M, Pins GD. The influence of microtextured basal lamina analog topography on keratinocyte function and epidermal organization. Journal of Biomedical Materials Research Part A. 2005; 72:47–56. [PubMed: 15543632]
30. Elsdale T, Bard J. Collagen substrata for studies on cell behavior. J Cell Biol. 1972; 54:626–37. [PubMed: 4339818]
31. Cornwell KG, Downing BR, Pins GD. Characterizing fibroblast migration on discrete collagen threads for applications in tissue regeneration. J Biomed Mater Res A. 2004; 71:55–62. [PubMed: 15368254]
32. Lu W, Miyazaki K, Mizushima H, Nemoto N. Immunohistochemical distribution of laminin-5 gamma2 chain and its developmental change in human embryonic and foetal tissues. Histochem J. 2001; 33:629–37. [PubMed: 12197671]
33. Zapatka M, Zboralski D, Radacz Y, Bockmann M, Arnold C, Schoneck A, et al. Basement membrane component laminin-5 is a target of the tumor suppressor Smad4. Oncogene. 2007; 26:1417–27. [PubMed: 16953227]
34. Maas-Szabowski N, Shimotoyodome A, Fusenig NE. Keratinocyte growth regulation in fibroblast cocultures via a double paracrine mechanism. J Cell Sci. 1999; 112 (Pt 12):1843–53. [PubMed: 10341204]
35. Szabowski A, Maas-Szabowski N, Andrecht S, Kolbus A, Schorpp-Kistner M, Fusenig NE, et al. c-Jun and JunB antagonistically control cytokine-regulated mesenchymal-epidermal interaction in skin. Cell. 2000; 103:745–55. [PubMed: 11114331]
36. Werner S, Smola H. Paracrine regulation of keratinocyte proliferation and differentiation. Trends Cell Biol. 2001; 11:143–6. [PubMed: 11306276]
37. El Ghalbzouri A, Hensbergen P, Gibbs S, Kempenaar J, van der Schors R, Ponec M. Fibroblasts facilitate re-epithelialization in wounded human skin equivalents. Laboratory investigation; a journal of technical methods and pathology. 2004; 84:102–12.
38. Krejci NC, Cuono CB, Langdon RC, McGuire J. In vitro reconstitution of skin: fibroblasts facilitate keratinocyte growth and differentiation on acellular reticular dermis. J Invest Dermatol. 1991; 97:843–8. [PubMed: 1717611]
39. Erdag G, Sheridan RL. Fibroblasts improve performance of cultured composite skin substitutes on athymic mice. Burns: journal of the International Society for Burn Injuries. 2004; 30:322–8. [PubMed: 15145189]
40. El Ghalbzouri A, Lamme E, Ponec M. Crucial role of fibroblasts in regulating epidermal morphogenesis. Cell and tissue research. 2002; 310:189–99. [PubMed: 12397374]
41. el-Ghalbzouri A, Gibbs S, Lamme E, Van Blitterswijk CA, Ponec M. Effect of fibroblasts on epidermal regeneration. The British journal of dermatology. 2002; 147:230–43. [PubMed: 12174092]

42. Smola H, Thiekotter G, Fusenig NE. Mutual induction of growth factor gene expression by epidermal-dermal cell interaction. The Journal of cell biology. 1993; 122:417–29. [PubMed: 8320264]
43. El Ghalbzouri A, Jonkman MF, Dijkman R, Ponec M. Basement membrane reconstruction in human skin equivalents is regulated by fibroblasts and/or exogenously activated keratinocytes. J Invest Dermatol. 2005; 124:79–86. [PubMed: 15654956]
44. Marionnet C, Pierrard C, Vioux-Chagnoleau C, Sok J, Asselineau D, Bernerd F. Interactions between fibroblasts and keratinocytes in morphogenesis of dermal epidermal junction in a model of reconstructed skin. J Invest Dermatol. 2006; 126:971–9. [PubMed: 16528360]
45. Aumailley M, Bruckner-Tuderman L, Carter WG, Deutzmann R, Edgar D, Ekblom P, et al. A simplified laminin nomenclature. Matrix Biol. 2005; 24:326–32. [PubMed: 15979864]
46. Burgeson RE, Christiano AM. The dermal-epidermal junction. Curr Opin Cell Biol. 1997; 9:651–8. [PubMed: 9330868]
47. Baker SE, Hopkinson SB, Fitchmun M, Andreason GL, Frasier F, Plopper G, et al. Laminin-5 and hemidesmosomes: role of the alpha 3 chain subunit in hemidesmosome stability and assembly. J Cell Sci. 1996; 109 (Pt 10):2509–20. [PubMed: 8923212]
48. Miyazaki K. Laminin-5 (laminin-332): Unique biological activity and role in tumor growth and invasion. Cancer Sci. 2006; 97:91–8. [PubMed: 16441418]
49. Fine JD, Eady RA, Bauer EA, Briggaman RA, Bruckner-Tuderman L, Christiano A, et al. Revised classification system for inherited epidermolysis bullosa: Report of the Second International Consensus Meeting on diagnosis and classification of epidermolysis bullosa. J Am Acad Dermatol. 2000; 42:1051–66. [PubMed: 10827412]
50. Meng X, Klement JF, Leperi DA, Birk DE, Sasaki T, Timpl R, et al. Targeted inactivation of murine laminin gamma2-chain gene recapitulates human junctional epidermolysis bullosa. J Invest Dermatol. 2003; 121:720–31. [PubMed: 14632187]
51. Nguyen BP, Ryan MC, Gil SG, Carter WG. Deposition of laminin 5 in epidermal wounds regulates integrin signaling and adhesion. Curr Opin Cell Biol. 2000; 12:554–62. [PubMed: 10978889]
52. Amano S, Akutsu N, Ogura Y, Nishiyama T. Increase of laminin 5 synthesis in human keratinocytes by acute wound fluid, inflammatory cytokines and growth factors, and lysophospholipids. Br J Dermatol. 2004; 151:961–70. [PubMed: 15541073]
53. Santoro MM, Gaudino G. Cellular and molecular facets of keratinocyte reepithelization during wound healing. Exp Cell Res. 2005; 304:274–86. [PubMed: 15707592]
54. Rosenberger C, Solovan C, Rosenberger AD, Jinping L, Treudler R, Frei U, et al. Upregulation of hypoxia-inducible factors in normal and psoriatic skin. The Journal of investigative dermatology. 2007; 127:2445–52. [PubMed: 17495954]
55. O'Toole EA, Marinkovich MP, Peavey CL, Amieva MR, Furthmayr H, Mustoe TA, et al. Hypoxia increases human keratinocyte motility on connective tissue. The Journal of clinical investigation. 1997; 100:2881–91. [PubMed: 9389755]
56. Rumpler M, Woesz A, Dunlop JW, van Dongen JT, Fratzl P. The effect of geometry on three-dimensional tissue growth. Journal of the Royal Society, Interface/the Royal Society. 2008; 5:1173–80.

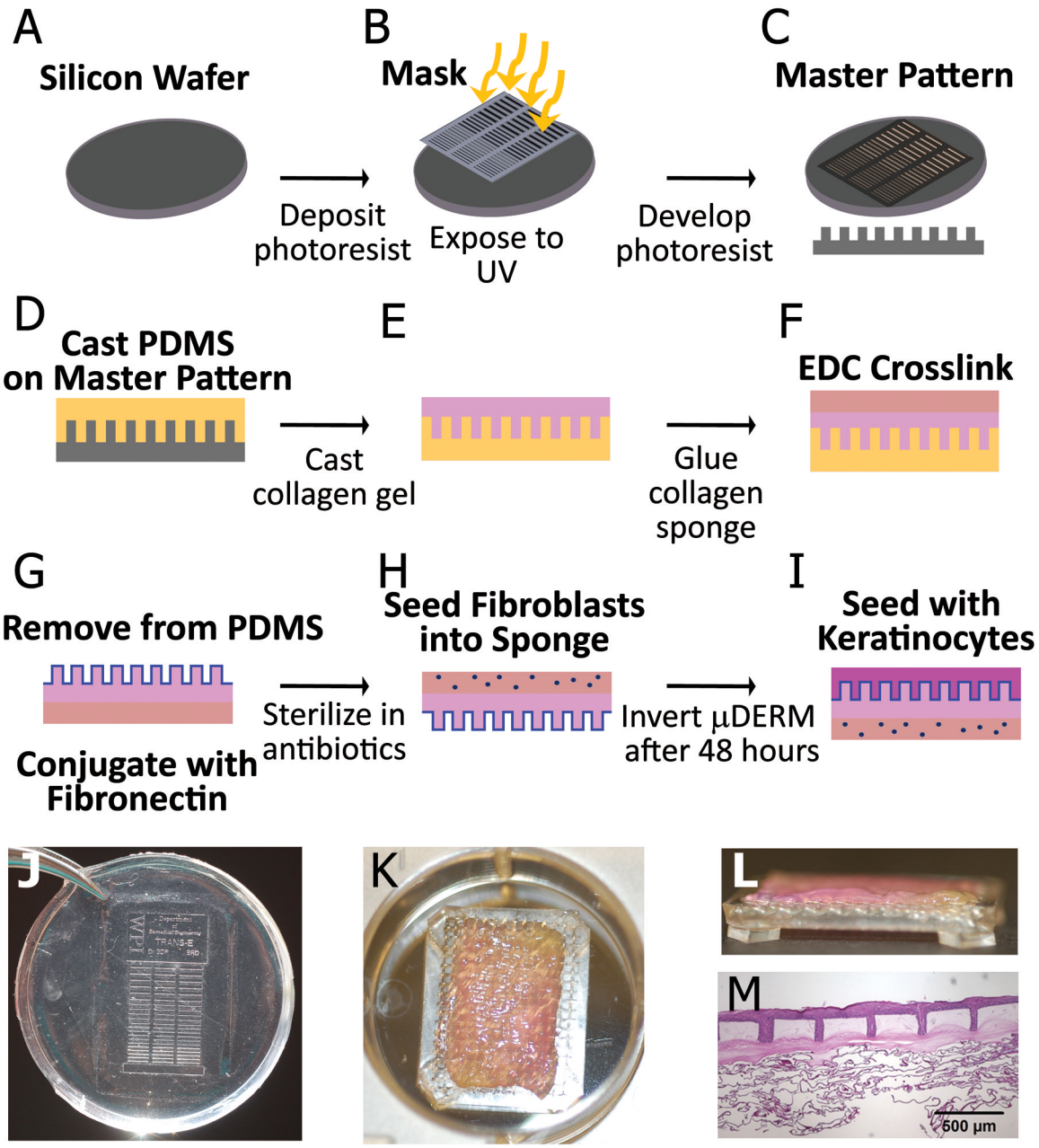

Figure 1.

Production of µDERM and 3D skin model system. Photolithography was used to create a silicon wafer with microtopographic features resembling the DEJ (**A–C**). Polydimethylsiloxane silicone elastomer (PDMS, 10:1 base to curing agent; Sylgard184; Dow Corning) was cured on the wafer's surface creating a negative mold (**D**). Type I collagen was self-assembled on the micropatterned molds (**E**) and a collagen-GAG sponge was laminated to the collagen matrix, and crosslinked to form the µDERM (**F**). µDERMs were conjugated with fibronectin (FN, 32 µg/cm^2; BD Biosciences) and sterilized (**G**). The dermal side was seeded with fibroblasts and for 48 hours (**H**) then the micropatterned epidermal surface was seeded with keratinocytes (**I**). After 48 hours, µDERMs were cultured at the air-liquid interface. **(J)** Photograph of PDMS pattern used to create µDERMs.

The collagen gel was cast over the entire area of the patterns, which were designed to fit into 6 well plates. **(K)** μDERM (collagen gel side up) on cell seeding screen in a 6 well plate. After removal from patterns, μDERMs were trimmed to 1.25cm × 2.0 cm and placed on cell-seeding screens. **(L)** Side view of μDERM on cell-seeding screen. Screens enable air-liquid interface culture. **(M)** Low magnification image of μDERM after 7 days of air-liquid culture.

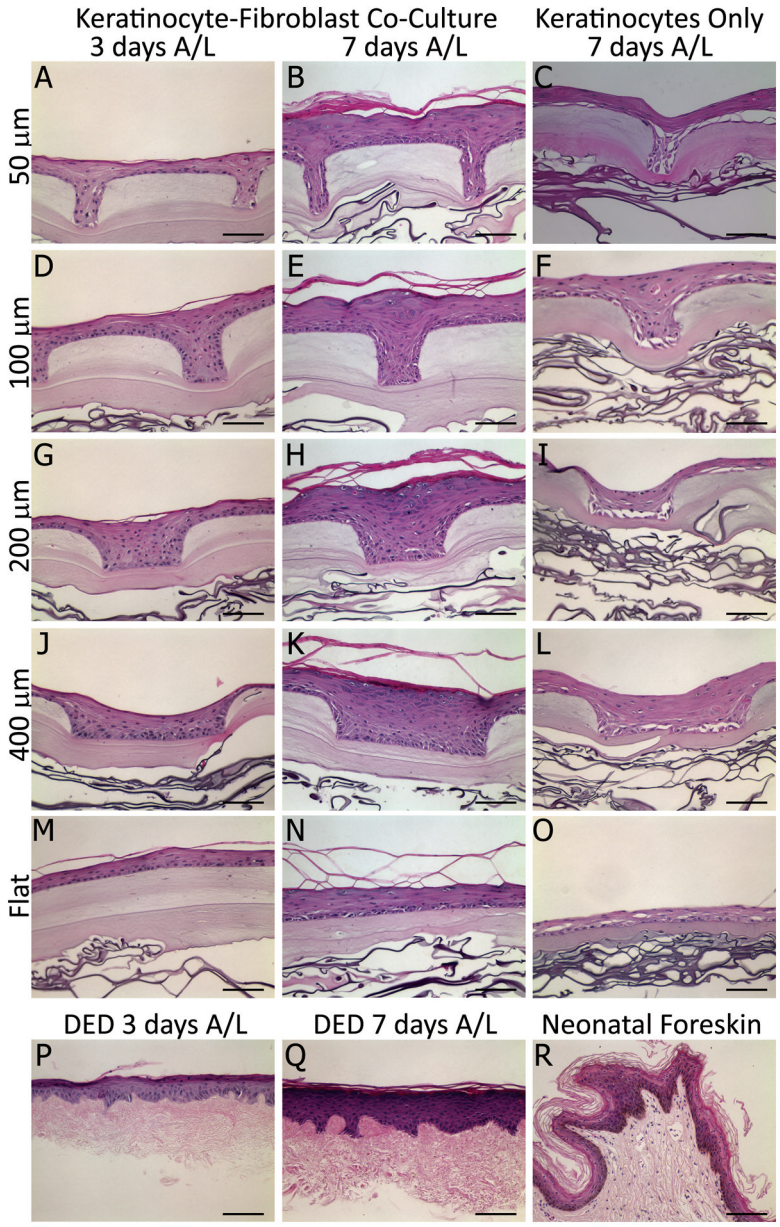

Figure 2.

Hematoxylin and eosin stain of cultured µDERMs. Keratinocytes cultured on µDERM form a stratified epidermis. µDERMs containing fibroblasts exhibit epidermal organization at 3 days (**A, D, G, J**). At 7 days, epidermal thickness is increased and distinct basal, spinous, granular, and cornified layers are observed (**B, E, H, K**). At both 3 and 7 days, µDERMs containing fibroblasts resemble DED controls (**P, Q**) and 7 day cultures are morphologically similar to neonatal foreskin controls (**R**). Keratinocytes cultured on flats (**M, N**) stratify, but lack a defined stratum granulosum present in microtopographies. Additionally, epidermal thickness is increased by channel topographies. In contrast, µDERMs cultured without fibroblasts (**C, F, I, L, O**) are characterized by a disrupted basal and suprabasal layers as well as poor epidermal stratification and differentiation. Scale bar = 100µm.

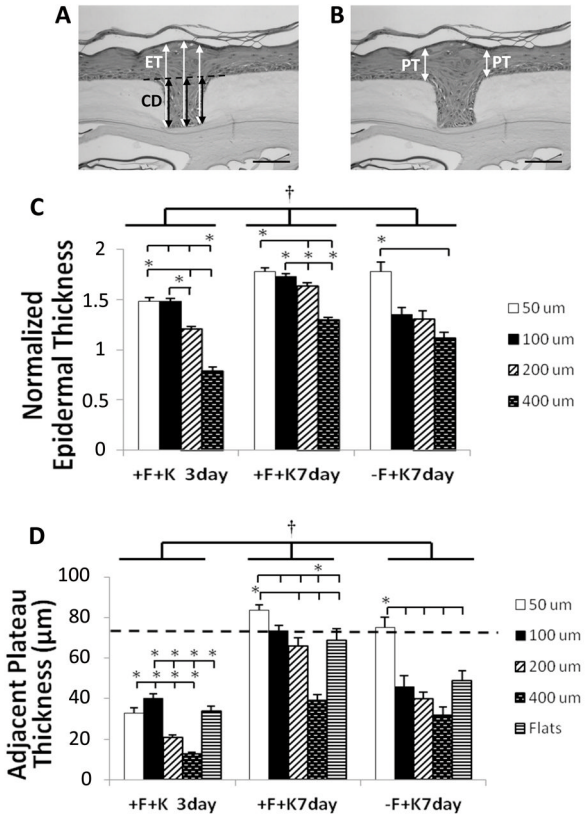

Figure 3. Morphometric analyses of epidermal thickness in keratinocyte microniches

Epidermal thickness (ET) is increased in narrow channel topographies. Epidermal thickness was normalized by dividing by channel depth (CD); three measurements were taken per well and averaged (**A**). Normalized epidermal thickness (**C**) increased from days 3 to 7 and by co-culture with fibroblasts, independent of topography. Additionally, normalized epidermal thickness in narrow channels is statistically increased compared to wider channels cultured under the same conditions. This difference is most pronounced on μDERMs cocultured with fibroblasts. Plateau thickness (PT) was measured immediately adjacent to each channel topography (**B**) and in the center of control flats. Plateau thickness increased adjacent to narrow channels and decreased adjacent to wide channels relative to flats (**D**). Data presented as mean±SEM. †indicates statistical difference between groups, $p<0.05$. * indicates statistical difference between indicated channel dimensions, $p<0.05$. Scale bar = 100μm.

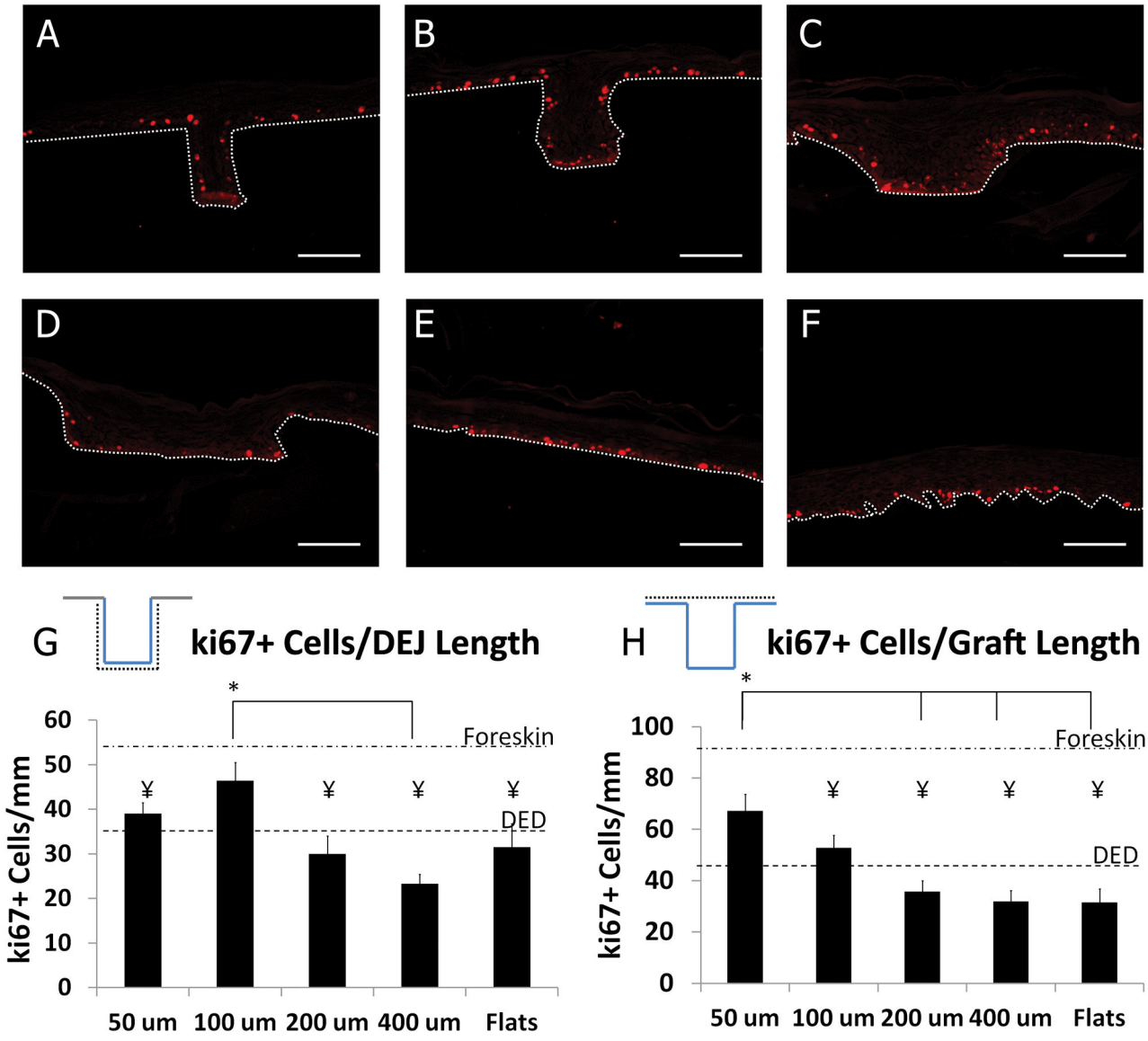

Figure 4. Proliferation on µDERM

Representative images of ki67 expression on µDERMs with 50µm (**A**), 100µm (**B**), 200µm (**C**), and 400µm (**D**) channels, on flat µDERM (**E**) and on DED (**F**). Dotted white line indicates DEJ. The linear density of ki67+ keratinocytes was calculated by normalizing against DEJ length (**G**) and planar graft length (**H**). Ki67+ cell density along the length of the DEJ within 100 µm channels is increased compared to 200 µm channels, 400 µm channels and flats. Ki67+ cell density along the length of the graft is significantly increased in regions containing 50 µm channels compared to 200 µm channels, 400 µm channels, and flats. Additionally, the graft density of ki67+ cells in narrow channeled regions is not statistically different from native foreskin. Scale bar = 100µm. Data presented as Mean ±SEM. * denotes statistical differences between specified microniche dimensions, ¥ indicates statistical difference from foreskin control, $p<0.05$.

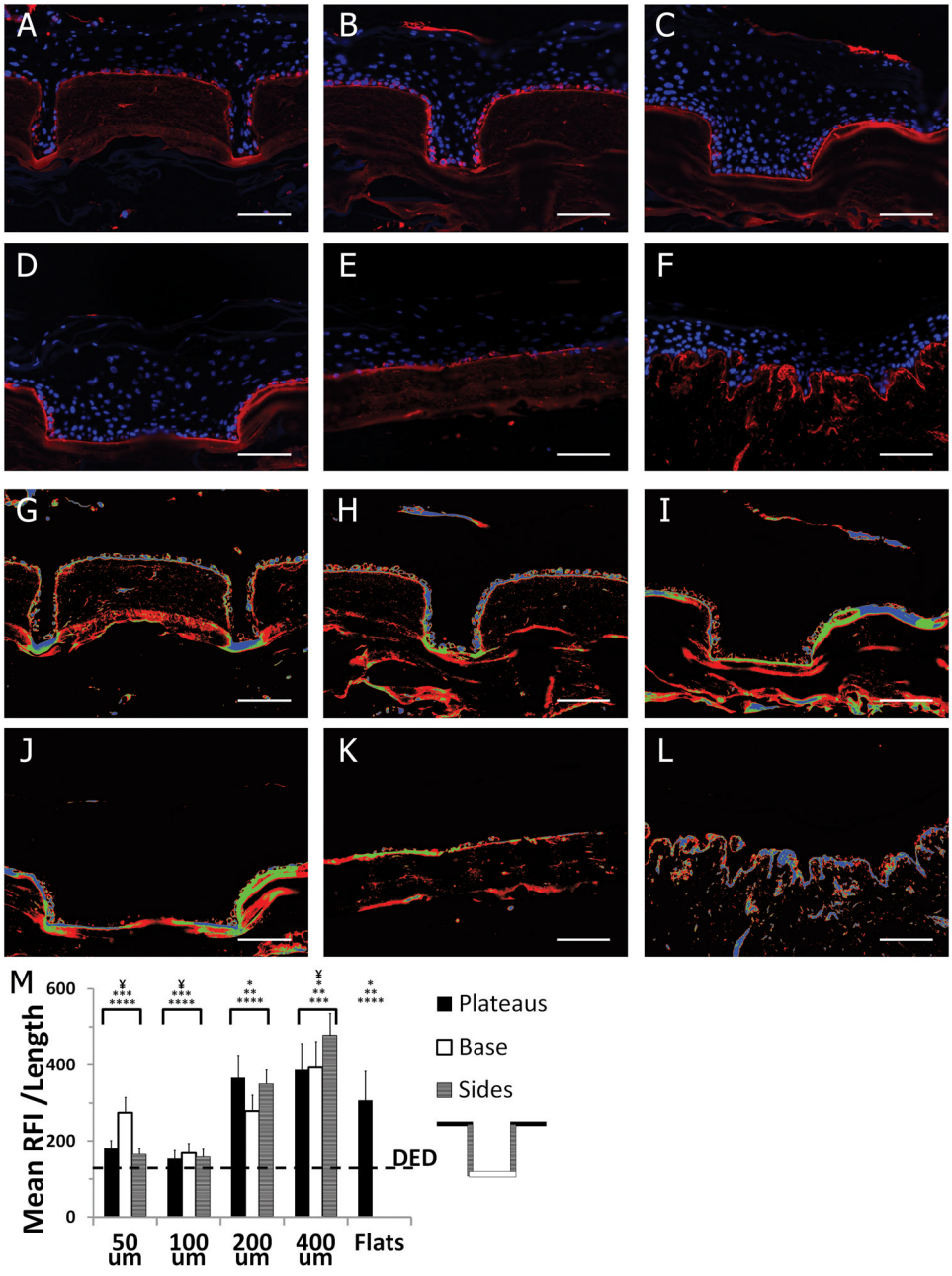

Figure 5. Basement membrane protein deposition on μDERM

Representative images of laminin-332 expression (Alexafluor546) on cultured μDERMs with 50μm (**A**), 100μm (**B**), 200μm (**C**), and 400μm (**D**) channels, on flat μDERM (**E**) and on DED (**F**). LUT false colorization of laminin 332 expression (**G–L**); blue = highest 1/3 laminin γ2 expression, green = mid 1/3 laminin γ2 expression, red = lowest 1/3 laminin γ2 expression. Laminin deposition was quantified by normalizing the relative fluorescent intensity (RFI) of 2 expression at the DEJ against DEJ length (**M**). Laminin 332 deposition is increased in wider channels and decreased in narrow channels compared to flat control features. There was no statistical difference in regional expression of laminin-332 within microniches (plateaus, channel base, channel sides) of a specific dimension. Data presented as mean ±SEM. c. Asterisks indicate statistical difference from: *50 μm channels, **100μm

channels, *** 200μm channels, ****400μm channels. ¥ Indicates statistical difference from flats control, $p<0.05$.

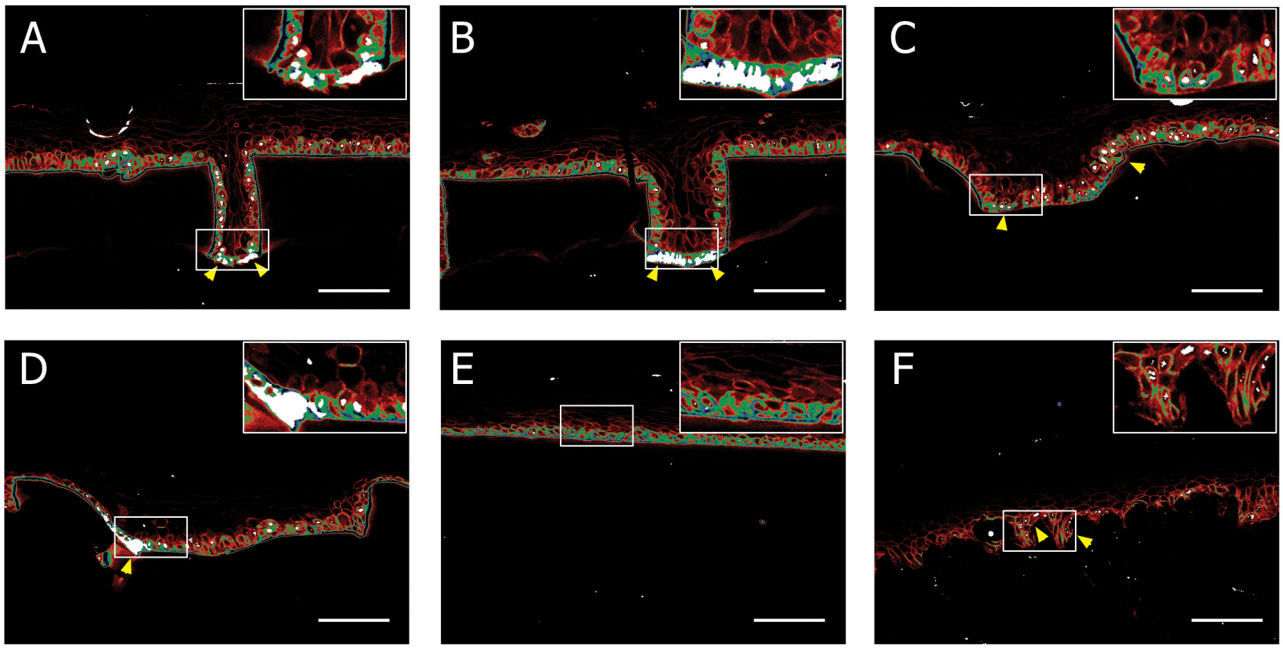

Figure 6. Cellular Localization on μDERM

LUT false colorization of β_1 integrin and p63 expression with 50μm (**A**), 100μm (**B**), 200μm (**C**), and 400μm (**D**) channels, on flat μDERM (**E**) and on DED (**F**); blue = highest 1/3 β_1 expression, green = mid 1/3 β_1 expression, red = lowest 1/3 β_1 expression, white = $p63^+$ nuclei. Insets show indicated regions of interest at high magnification. $\beta_1^{bri}p63^+$ keratinocytes preferentially localize to the bases of 50μm (**A**) and 100μm (**B**) channels and the corners of 400μm channels (**D**). In contrast, β_1^{bri} cells are randomly distributed on flat regions and p63 expression is limited. On DED, $\beta_1^{bri}p63^+$ cells are located in niches (**F**). Scale bar = 100μm.